A Novel Zero-Insertion-Force (ZIF) Micro (μ)-Connector: Design, Fabrication, and Measurements

Ben-Hwa Jang, Hsin-Yu Huang, and Weileun Fang, *Member, IEEE*

***Abstract*—This paper presents the design, fabrication, and measured properties of a novel zero-insertion-force (ZIF) micro (μ)-connector. The proposed ZIF μ-connector is shown to remedy a number of problems in the existing microelectromechanical-system-based connectors, such as the wearing effect, the poor signal integrity for high-speed signal transmission, and the lack of latch design. The three-mask and silicon-on-insulator wafers are designed for the simultaneous fabrication of terminals and latches. Prototype connectors are demonstrated with five 1800-μm-long, 100-μm-wide, and 2-μm-high terminals on a 150-μm pitch. The terminals and latches are actuated by electrostatic force to avoid the wearing and kinking during the mating process. The terminal is a multimorph cantilever to form a hooklike out-of-plane shape. The controlled shape of the terminal provides a reliable contact at the interface. The properties of the proposed ZIF μ-connector are measured and analyzed, including the out-of-plane shape of the terminal, driving voltage, dc contact resistance, and the RF characteristics. The potential applications of the ZIF μ-connector include the fine-pitch high-speed interconnection, 3-D reworkable packaging, and the performance enhancement of many existing μ-connectors.**

***Index Terms*—Microelectromechanical systems (MEMS) connectors, out-of-plane shape control, zero insertion force (ZIF).**

I. Introduction

ACTING AS THE connecting components among electronic devices, connectors have been extensively employed in industries for many years [1], [2]. Since there is an increasing demand for more challenging specifications, many methods based on the microelectromechanical systems (MEMS) technology have been reported to extend the scope of miniaturization at a potentially lower cost. Unno *et al.* [3] presented a fork-type micro (μ)-connector by using UV thick photoresist (PR) and Ni electroforming to attain the features of finer pitch and higher package density. Toshiyoshi *et al.* [4] patterned fringes of chip into pin shapes to integrate various kinds of microchips independent of material or fabrication compatibility. The pin-shaped fringe of chip was coated with Cr/Au for low contact resistance, and it can be vertically inserted into the micromotherboard for electrical and physical connections. Tracy *et al.* [5] developed a bone-wire scale method of fabricating connectors, providing the features of fine pitch, low profile, and high pin counts. Miller *et al.* [6] reported a high-density μ-connector array fabricated using the flip-chip assembly. The internal residual stress of gold was used to form the out-of-plane shape of terminals, and the connection of the electrical signal was controlled by the electrostatic actuation. Larsson *et al.* [7]–[9] presented an in-line separable electrical connector fabricated by the micromachining process with nonplanar terminals and a self-aligning mechanical structure. The wear and thermal tolerance of contact resistance was improved by using the hard Co–Au alloy and by rearranging the constituent conductor layers to balance thermal stresses.

In spite of various improvements brought by the aforementioned methods, many issues remain to be addressed. For example, the wearing effect is inevitably produced at the contact interface of the terminals during the mating and demating processes, causing the degradation of signal transmission and the life of connectors [2], [10], [11]. The shielding of electromagnetic interference (EMI) is yet another issue to be addressed for connectors fabricated by the MEMS technology. Moreover, the performances of MEMS connectors are also influenced by the problems of lacking proper impedance-matching design, as well as latching mechanism. To improve the performances of MEMS connector, this paper presented an innovative zero-insertion-force (ZIF) (μ)-connector. The design and fabrication issues were addressed, and its properties were quantitatively evaluated. The proposed ZIF μ-connector has many applications such as the fine-pitch interconnection, 3-D reworkable packaging, and the test platform for MEMS devices.

II. ZIF μ-Connector Design

Fig. 1(a) shows a schematic diagram of the proposed ZIF μ-connector. It consisted of two major components: the *receptacle* and *plug*. The receptacle can be further decomposed into a cap on the top, and a base with five terminals and two latches at the bottom. The base was designed on a sandwichlike silicon-on-insulator (SOI) wafer, as shown in Fig. 1(b), where the

Manuscript received August 8, 2008; revised October 28, 2008. First published December 2, 2008; current version published April 1, 2009. This work was supported in part by the National Science Council of Taiwan under Grant 95-2218-E-007-024 and in part by the Ministry of Economic Affairs of Taiwan under Grant 7354DB2210.

B.-H. Jang is with the Institute of NanoEngineering and MicroSystems, National Tsing Hua University, Hsinchu 30013, Taiwan, and also with the Material and Chemical Research Laboratories, Industrial Technology Research Institute, Hsinchu 31040, Taiwan (e-mail: benhwa@itri.org.tw).

H.-Y. Huang is with the Department of Power Mechanical Engineering, National Tsing Hua University, Hsinchu 30013, Taiwan (e-mail: d947728@oz.nthu.edu.tw).

W. Fang is with the Institute of NanoEngineering and MicroSystems and the Department of Power Mechanical Engineering, National Tsing Hua University, Hsinchu 30013, Taiwan (e-mail: fang@pme.nthu.edu.tw).

Color versions of one or more of the figures in this paper are available online at http://ieeexplore.ieee.org.

Digital Object Identifier 10.1109/TIE.2008.2010086

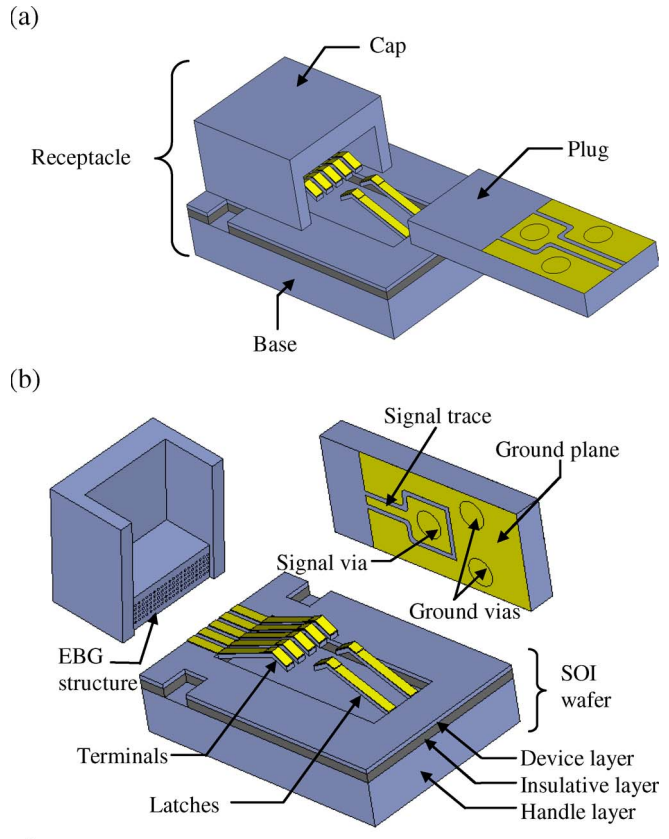

Fig. 1. Schematic diagram of (a) the assembled μ-connector and its perspective view and (b) components consisting of the μ-connector.

conductive silicon device and handle layers are isolated by the silicon dioxide insulative layer. The terminals and the latches were implemented using the device layer of the SOI wafer. The out-of-plane shapes of the terminals and latches were controlled by using the residual stresses of the deposited films. This hooklike shape provides the suitable contact normal force at the contact interface and the locking force for the latches. The silicon cap was disposed over the base and provided periodical cylinder holes to form an electromagnetic bandgap (EBG) structure, enabling the EMI shielding and the enhanced rigidity of the cap [12], [13]. Some marks were designed on the base for the ease of the cap and base assembly. After the cap being precisely placed on the base, the gel was pasted around the surrounding cap, and then, these two components were bonded together. The plug was implemented on a chip containing different microcomponents, such as the CMOS circuit, the MEMS device, the integrated passive device, or other alternatives. In this paper, the simple ground–signal–ground (GSG)-type electrical traces were routed on both sides of the plug to demonstrate the electrical performance of the proposed ZIF μ-connector. The electrical traces were interconnected by the signal via and the ground vias.

The thin film deposited onto the terminal due to residual stress may cause the terminal to bend downward or upward. If the terminal bends downward, as shown in Fig. 2(a), the electrical signals cannot be transmitted efficiently when the plug is inserted into the receptacle. On the other hand, if the terminal bends upward, as shown in Fig. 2(b), the terminal may be

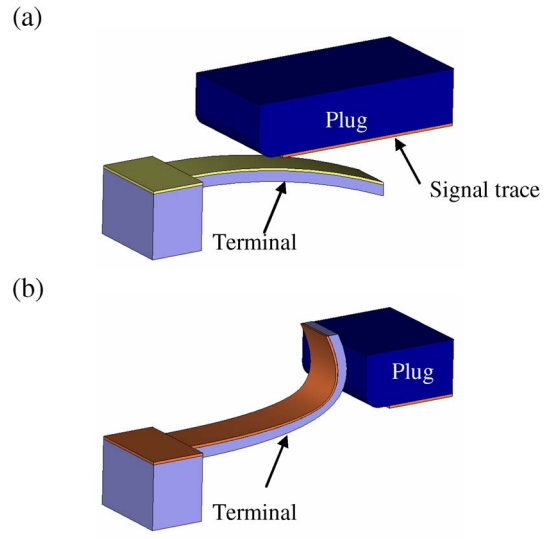

Fig. 2. (a) Terminal bends downward and the electrical signals cannot be transmitted when the plug is inserted into the receptacle. (b) Terminal bends upward and the terminal may be broken when the plug is inserted (the kinking effect).

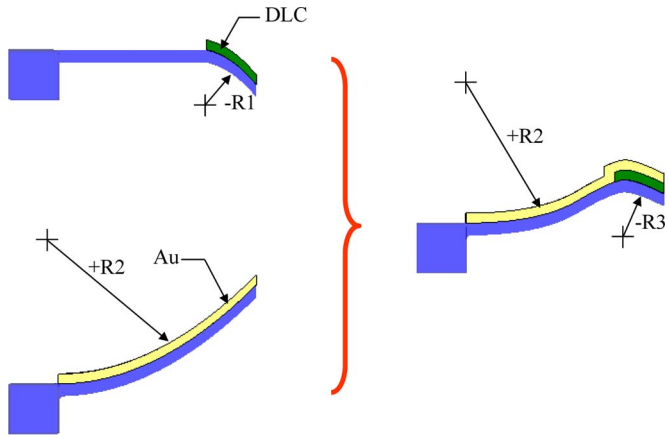

Fig. 3. Illustration of the mechanism of the out-of-plane shape of the terminal.

broken when the plug is inserted, known as the kinking effect. In short, the shape of terminal will determine the condition of contact interface and further influence the quality of signal transmission. This paper presented the terminal design with a hooklike shape to ensure the stability of signal transmission and the prevention of the open circuit at the contact interface. The terminal was a multimorph cantilever, and its out-of-plane shape was controlled using the thin film residual stresses, as shown in Fig. 3. In short, the beam tip was bent down with a radius of curvature $-R1$ using a compressive diamondlike carbon (DLC) film. After that, the whole cantilever was bent by a gold film with residual tension. Thus, the terminal tip formed by the Au–DLC–Si trimorph had a radius of curvature of $-R3$. In addition, the rest portion of the terminal consisted of the Si–Au bimorph had a radius of curvature $R2$, so as to form the hooklike shape.

The concept of ZIF was employed to prolong the life cycle of μ-connectors by eliminating the kinking effect. The mechanism of ZIF is shown in Fig. 4. As shown in Fig. 4(a), the terminal and latch can be bent downward from their initial positions

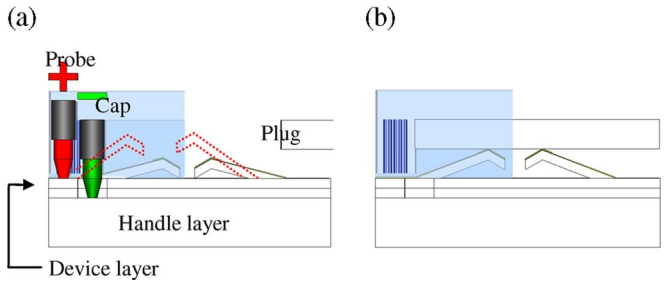

Fig. 4. Illustration of the mechanism of ZIF. (a) Apply a voltage through the device and handle layers, and force the terminals and latches to be bent downward. (b) Insert the plug, and remove the voltage.

(as indicated by the dashed line) by means of the electrostatic force. Thus, the wearing and kinking problems resulting from the insertion of plug into the receptacle can be prevented. As shown in Fig. 4(b), the terminal and latch will bounce back to their initial positions after removing the electrostatic force. Consequently, the terminal was then electrically connected with the traces routing on the plug, and the latch provided suitable retaining force for the plug and the receptacle assembly.

III. ZIF μ-Connector Fabrication

A three-mask process, as shown in Fig. 5, was developed to fabricate the base of the μ-connector. In order to reduce the coupling interference for the high-speed signal transmission, an SOI wafer with a high resistivity [(HR); $> 3000\ \Omega \cdot$ cm] was used for the base fabrication, as shown in Fig. 5(a). As shown in Fig. 5(b), the Al layer evaporated by the electron beam was patterned to act as the hard mask for the following Si etching by deep reactive ion etching (DRIE). The chemistries used in the DRIE process were sulfur hexafluoride (SF_6) for the etch step and C_4F_8 source gas for the passivation step, respectively [14]. The terminals and latches were then defined on the device Si layer. The dimensions of the SOI wafer and the terminals/latches are listed in Table I. As shown in Fig. 5(c) and (d), a PR layer of the device layer was patterned by using a negative photolithography process followed by the deposition of a 300-nm-thick DLC film. The ion plating with the pulsed cathodic vacuum laser arc was used at the -100-V bias, 20-μs pulse-on time, and 5% duty cycle. Here, the duty cycle is given by [15]

$$\text{Duty Cycle} = \frac{\text{pulse-on time}}{\text{pulse-on time} + \text{pulse-off time}} \times 100\%.$$

Under these conditions, the wafer heated by the ion bombardment during the deposition could be maintained around 100 °C. It is well below the baking temperature of the PR at 125 °C. Subsequently, the DLC was patterned on the Si device layer by using the lifting_off process. Such DLC film rendered the required compressive residual stress and a strong adhesion to the silicon surface. Similarly, the Au/Cr films were deposited and patterned using the liftoff process, as shown in Fig. 5(e) and (f). The Au/Cr films were covered on the whole terminals/latches by using the electron beam evaporation method to act as the conducting layer. In addition, the Au/Cr films (Cr with

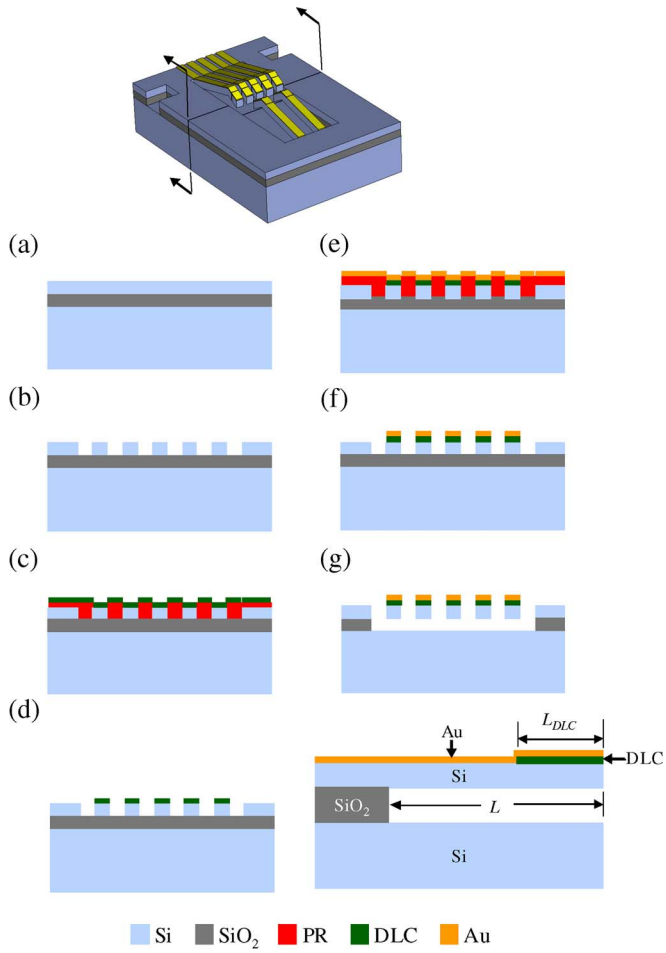

Fig. 5. Fabrication process for the base. (a) Use HR SOI wafer. (b) Pattern the device layer for terminals and latches by DRIE. (c) Spin coat and pattern PR, and then, deposit DLC. (d) Lift PR off. (e) Spin coat and pattern PR, and then, deposit Au. (f) Lift PR off. (g) Etch the insulator layer by HF solution, and release terminals and latches.

a thickness of 30 nm) provided the required tensile residual stress to control the shape of the terminal. Finally, the terminals and latches were released from handling Si substrate after the sacrificial oxide layer underneath was removed by HF, as shown in Fig. 5(g). Thus, the hooklike shape terminal was achieved. As indicated in the side view of Fig. 5(g), the Si terminal of length L has a deposited DLC film of length L_{DLC}.

Fig. 6 shows the fabrication process of the cap and the plug, respectively. The silicon wafer with a thickness of 1000 μm was used to fabricate the cap, as shown in Fig. 6(a). The Al film with a thickness of 300 nm was patterned on the wafer to act as a hard mask. The 700-μm deep cavity and trenches were defined by DRIE on the cap substrate. These trenches were used to form the EBG structure. The planar dimensions for the EBG structure were $50\ \mu\mathrm{m} \times 50\ \mu\mathrm{m}$ with a pitch of 50 μm. Fig. 6(b) shows the fabrication process of the plug. The 300-μm-thick PR was patterned on both sides of the high-resistivity silicon wafer. The 200-nm-thick Cr/Au films were patterned using the liftoff process to act as the electrical traces on the plug. The through-wafer vias with a diameter of 300 μm were fabricated by DRIE, and the Al film was used as the hard mask. After the removal of the Al, the Ag paste was filled into the vias by a

TABLE I
STRUCTURAL GEOMETRY OF THE ZIF μ-CONNECTOR

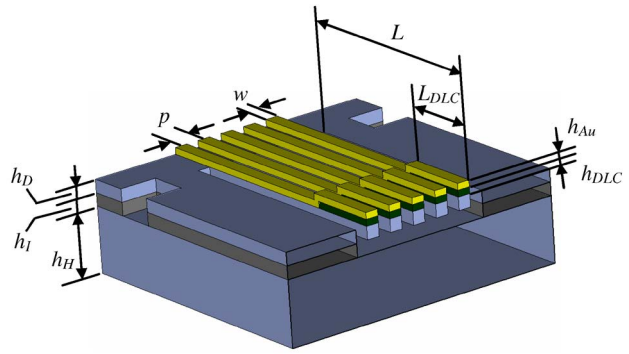

Parameter	Value	Unit	Description
L	1800	μm	Length of the terminal
L_{DLC}/L	5%, 10%, 20% 30%, 40%		Deposition ratio of DLC film
w	100	μm	Width of the terminal
p	150	μm	Pitch of the terminal
h_{Au}	0.3	μm	Thickness of Au
h_{DLC}	0.3	μm	Thickness of DLC
h_D	2	μm	Thickness of the device layer
h_I	4	μm	Thickness of the insulative layer
h_H	500	μm	Thickness of the handle layer

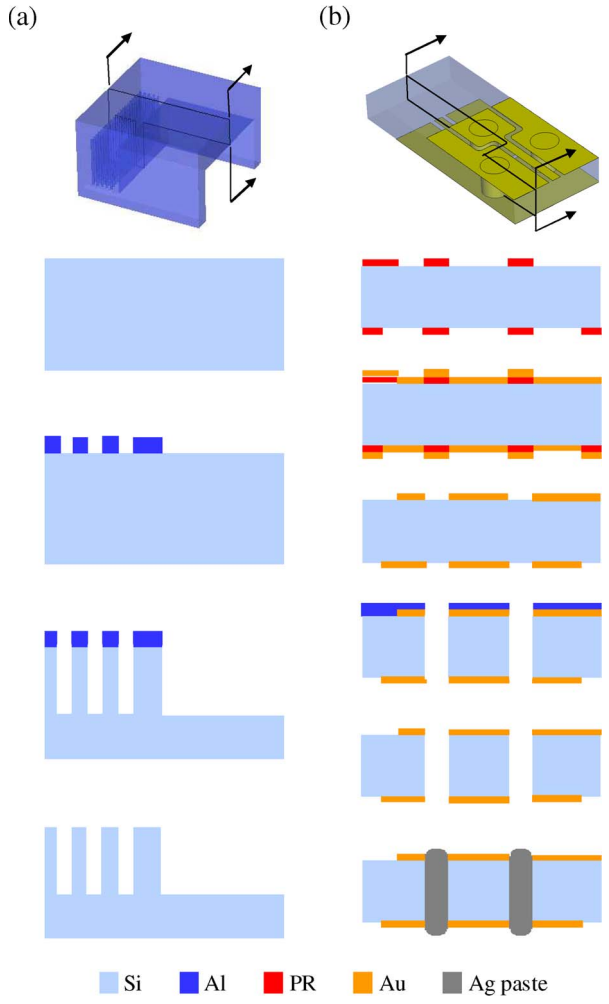

Fig. 6. Fabrication process for (a) the cap and (b) the plug.

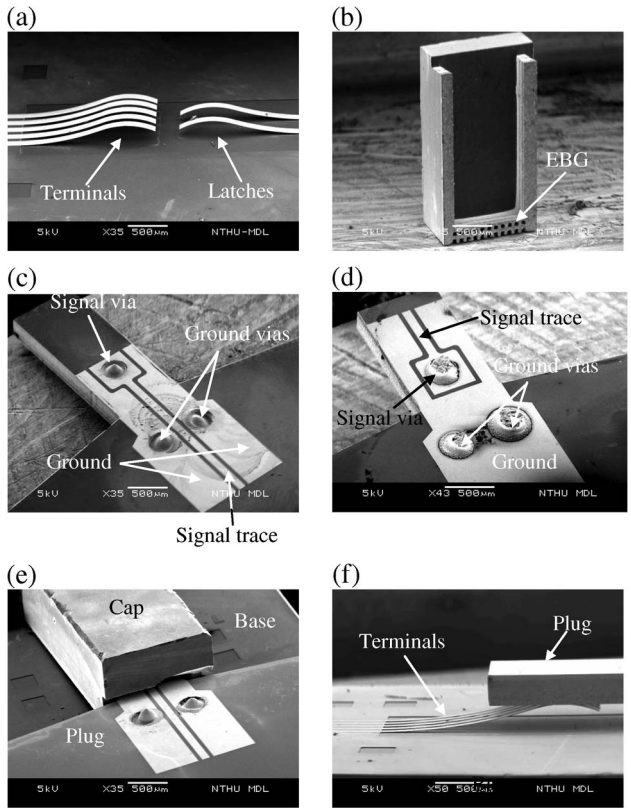

Fig. 7. SEM photomicrographs of the completed ZIF μ-connector components. (a) Terminals and latches. (b) Cap. (c) Top view of the plug. (d) Bottom view of the plug. (e) Assembly with the cap. (f) Assembly without the cap.

pneumatic dispensing system and heated and cured at 120 °C for 20 min to act as the through-wafer interconnects.

IV. EXPERIMENTAL RESULTS AND DISCUSSION

Fig. 7 shows the SEM micrographs of a typical fabricated ZIF μ-connector. The hooklike shape of five-way terminals and two-way latches can be clearly observed in Fig. 7(a). The SEM micrograph in Fig. 7(b) shows the fabricated cap with an EBG structure at the rear end of the cap. The top and bottom views of the plug are shown in Fig. 7(c) and (d), respectively. The GSG electrical traces and their vias are indicated in these two SEM micrographs. The assemblies of the ZIF μ-connector with and without cap are shown in Fig. 7(e) and (f), respectively. The SEM micrographs in Fig. 8 show the deflection profiles of the terminals for different deposition lengths L_{DLC} of DLC film. The terminal length L is 1800 μm, and the length ratio L_{DLC}/L as indicated in Fig. 5(g) ranges from 5% to 40%. These micrographs demonstrated the feasibility of altering the terminal to the expected shape by varying the deposition length L_{DLC}. Fig. 9 shows the measured out-of-plane profile of terminal at different length ratios L_{DLC}/L. The deflection of the terminals was measured by the three-axis measuring microscope with a linear encoder (OLYMPUS STM 6). The optical resolution is 100 nm. As a result, both the position and the profile of the terminal tip were significantly changed at different deposition lengths of DLC film. Thus, the performance of the connector can be modified.

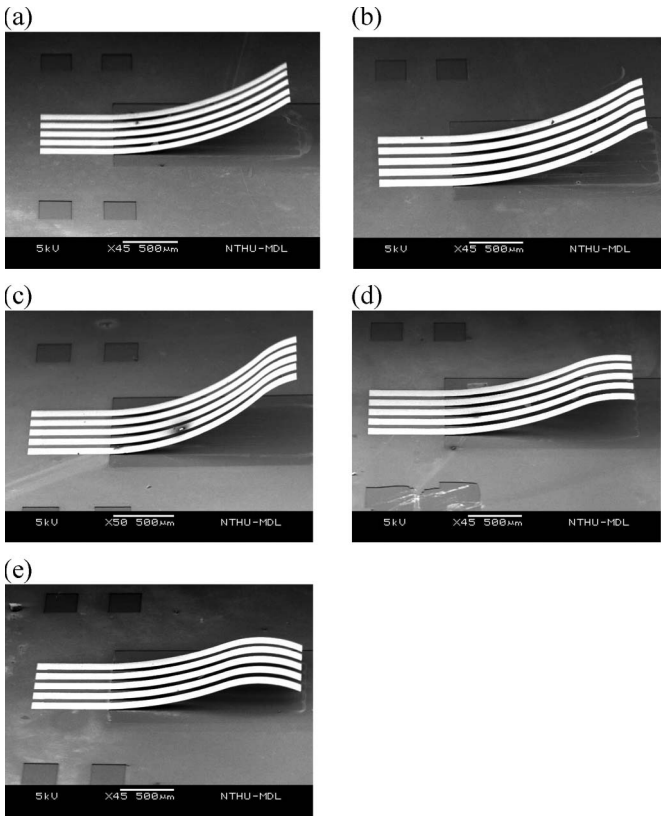

Fig. 8. SEM photomicrographs of the terminals with different deposition ratios ($L_{\rm DLC}/L$) of DLC. $L_{\rm DLC}/L =$ (a) 5%, (b) 10%, (c) 20%, (d) 30%, and (e) 40%.

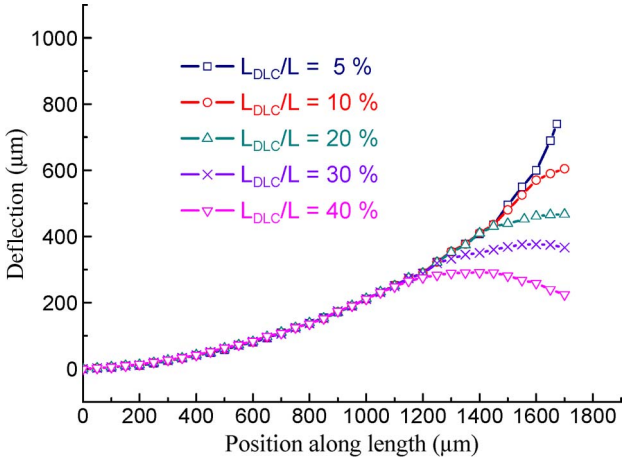

Fig. 9. Measured out-of-plane deflection profile along the length of the terminal with different deposition ratios of DLC.

The deflection of terminal driven by the electrostatic force was also characterized. The relationships between the actuation voltages and the tip deflections for the terminals with length ratios $L_{\rm DLC}/L$ of 5% and 40% are shown in Fig. 10(a) and (b), respectively. The measurement results in Fig. 10(a) indicate that the terminals with $L_{\rm DLC}/L$ of 5% required a driving voltage of 300 V to pull the terminal down, touching the handle layer of the SOI wafer. Due to the initial profile shown in Fig. 9, the terminal tip did not have contact with the surface of the handle

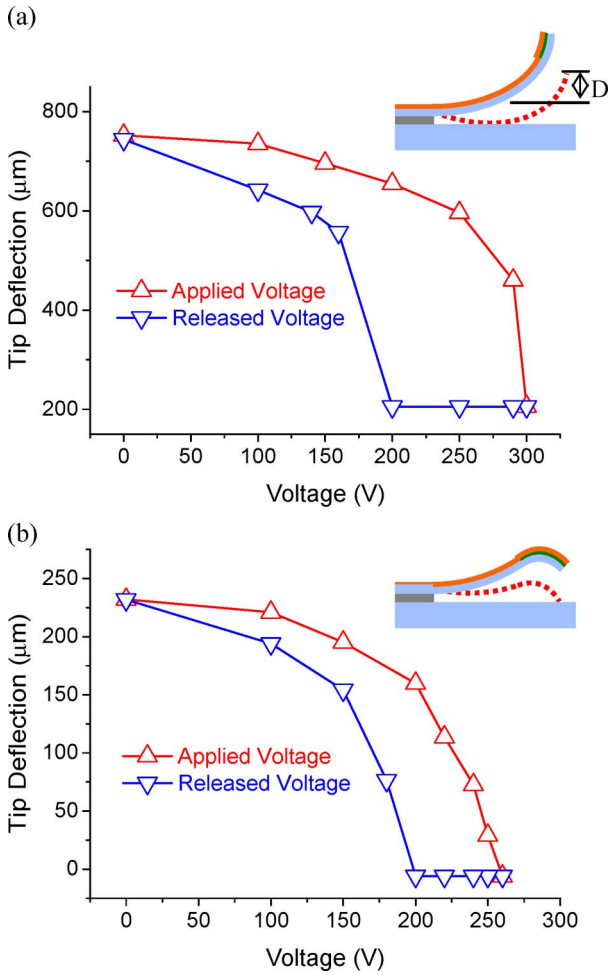

Fig. 10. Relationship between the actuated voltage and the tip deflection of the terminal with deposition ratio of DLC. (a) $L_{\rm DLC}/L = 5\%$. (b) $L_{\rm DLC}/L = 40\%$.

Si layer at a voltage of 300 V, as indicated by the dashed line in the inset of Fig. 10(a). Therefore, the tip deflection of terminal remained at $D = 205$ μm. On the other hand, the measurement results in Fig. 10(b) indicate that the terminals with $L_{\rm DLC}/L$ of 40% required a driving voltage of 260 V to pull the terminal down, touching the handle layer of the SOI wafer. In this case, the contact point was at the terminal tip while driving at 260 V, as indicated by the dashed line in the inset of Fig. 10(b).

The experimental setup shown in Fig. 11(a) was established to characterize the contact resistance of mated connectors. The total resistance of the circuit was measured using a micro-ohmmeter and the four-point probes. An equivalent circuit of the experimental setup is shown in Fig. 11(b), and the measured resistance can be expressed as

$$R_{\rm measured} = R_{\rm base} + R_{\rm plug} + R_C \tag{1}$$

where R_C represents the contact resistance at the contact interface, and $R_{\rm base}$ and $R_{\rm plug}$ are the equivalent bulk resistances on the base (including terminal) and the plug, respectively. The equivalent bulk resistance of $R_{\rm base} + R_{\rm plug}$ was estimated by using commercial electromagnetic-field simulation software (Ansoft Q3D Extraction, USA) for parasitic property

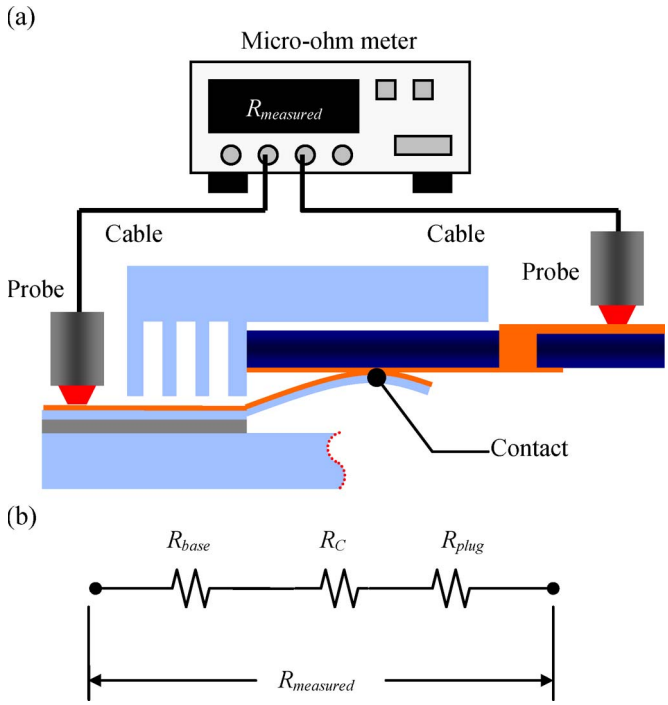

Fig. 11. (a) Experimental setup. (b) Equivalent circuit for measured contact resistance.

TABLE II
MATERIAL PROPERTIES USED IN THE ZIF μ-CONNECTOR MODEL FOR DC RESISTANCE AND RF CHARACTERISTIC SIMULATION

	Si	SiO_2	DLC	Au
Dielectric constant	11.9	4	7.5	
Loss tangent	0.005 @ 1GHz 0.015 @ 10GHz			
Conductivity (s/m)				4.1×10^7

TABLE III
MATERIAL PROPERTIES USED IN THE ZIF μ-CONNECTOR MODEL FOR NORMAL FORCE SIMULATION

	Si	DLC	Au
Young's modulus (GPa)	169	455.07	78
Poisson's ratio	0.28	0.17	0.44

The Young's modulus of DLC was measured by a nano-indenter.

extraction. The material properties used in the simulation are given in Table II. The simulated result indicated that the value of $R_{\rm base} + R_{\rm plug}$ was 3.28 Ω. Thus, with a typical measured resistance $R_{\rm measured}$ of 3.60 Ω, the contact resistance R_C can be extracted from (1) as $R_C = 0.32\ \Omega$.

In the case of the terminal's length being 1800 μm with the $L_{\rm DLC}/L$ of 40\%, the terminals had a typical displacement of 89 μm when the plug was inserted into the receptacle. Moreover, the terminal stiffness was determined using commercial finite element software (ANSYS, USA), and the material properties for simulation are listed in Table III. Since the thickness of the thin films deposited on the terminal is much thinner than that of the terminal, a symmetrical model along the width of the terminal was created to increase the simulation efficiency. Furthermore, the mapped mesh and high-order elements were used to improve the accuracy. As a result, the typical normal force at the contact point was extracted as 0.72 μN. Due to the small contact force, the contact resistance (several hundreds of milliohms) incurred by the proposed ZIF connector was one order higher than that in conventional microscale connectors (several tens of mO). It should be noted that the skin effect will affect the contact resistance at the high signal frequencies, and the contact resistance may induce a significant RF conductor loss as it exceeds the value of 1 Ω [11]. Thus, the proposed ZIF μ-connector is still suitable for RF applications.

To investigate the RF characteristics more thoroughly, the assembled ZIF μ-connector was probed on a probe station with an air coplanar GSG probe having a 150-μm pitch. The two-port RF characterization was performed up to a frequency of 9 GHz using the vector network analyzer (VNA). To calibrate the VNA directly at the probe tip interface, the commercial impedance standard substrate calibration kit (101–190 B, Cascade Microtech Inc.) and the standard short-open-load-through calibration method were used. The measured data were compared with the data predicted from the commercial electromagnetic-field solver (Ansoft HFSS, USA). A model of the simulated ZIF μ-connector is shown in Fig. 12(a), and the material properties used in the simulation are listed in Table II. In order to compare the simulation results with those from the measurements, the GSG ports were set at both ends. The port impedances at ports 1 and 2 were 50.8 and 51.7 Ω, respectively. The simulation frequency swept from dc to 10 GHz. The simulated surface current at 5 GHz is shown in Fig. 12(b). The insertion and return losses obtained from both measurement and simulation are shown in Fig. 12(c) and (d), respectively. The measured insertion losses at 5 and 9 GHz were 0.57 and 1.11 dB, respectively. The return loss was still below 10 dB, as the frequency was up to 9 GHz.

V. CONCLUSION

A novel ZIF μ-connector was designed and implemented in this paper. The three-mask process on SOI wafer design facilitated the easy fabrication of the terminals and latches simultaneously. The hooklike shape of the terminals was controlled by the residual stresses of deposited films. The Au deposited on the whole surface of the terminals bent the terminals up to prevent the open circuit at the contact interface after mating. The DLC deposited on the tip of the terminals bent the tips of the terminals down to enhance the reliable contact at the contact interface. This out-of-plane configuration can be shaped by varying the length of the DLC film. The hooklike shape of the terminals indeed affected the performance of the proposed ZIF μ-connector, such as the contact force, the contact resistance, and the actuated voltage for ZIF. In order to prevent the wearing and kinking effects, the terminals and latches were actuated by electrostatic force during the mating and demating processes. The proposed connector was possessed of larger dc

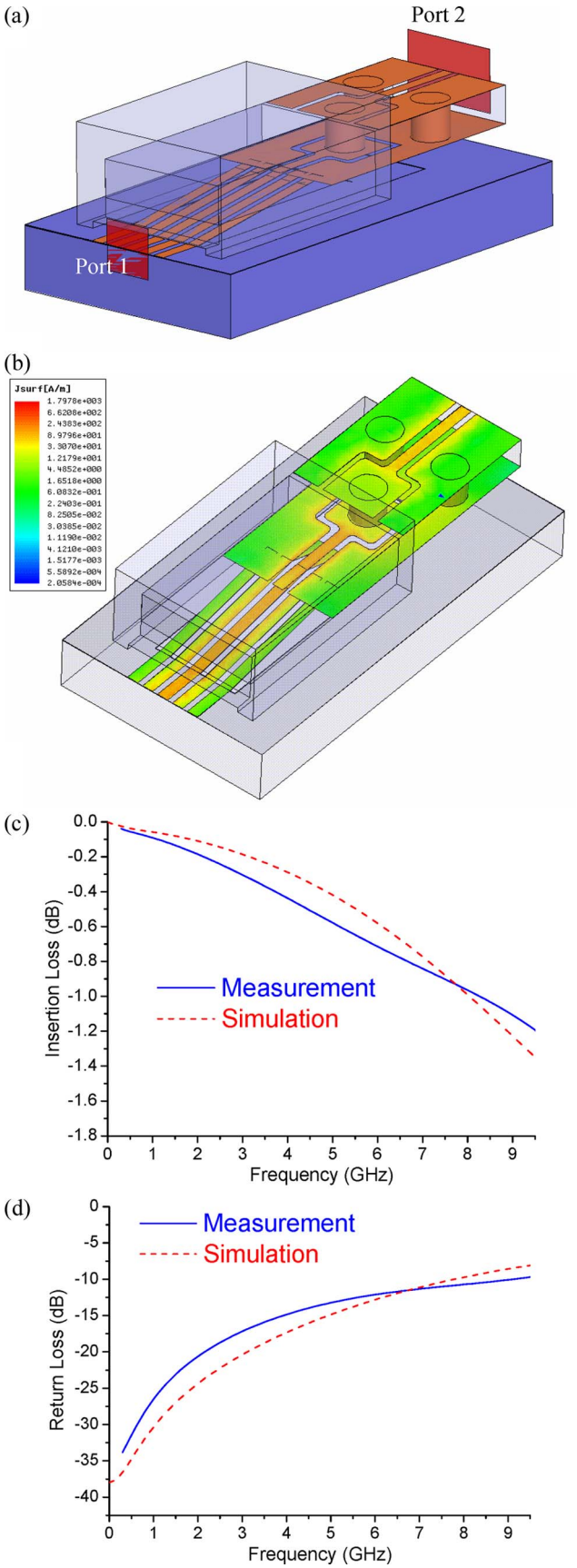

Fig. 12. (a) Three-dimensional model of mated ZIF μ-connector for RF property simulation showing port labeling convention, (b) the surface current at 5 GHz, and comparison between the simulated and measured (c) insertion loss and (d) return loss.

contact resistance compared with the one in traditional MEMS-based connectors due to the smaller normal contact force, but it was still suitable for RF application. Moreover, the proposed ZIF μ-connector possessed superior RF characteristics and therefore had good potentials for RF applications. The shielding effectiveness of the EBG structure on the cap can be further investigated. In order to achieve the optimal out-of-plane shape with specific applications, an analytical study seems to be beneficial and will be further explored in the future.

ACKNOWLEDGMENT

The authors would like to thank Dr. J.-B. Wu and C.-Y. Chen of the Material and Chemical Laboratories, Industrial Technology Research Institute, for providing the DLC plating fabrication of this paper. The access to the fabrication facilities, provided by the Center for Nano-Science and Technology, National Tsing Hua University; Nano Facility Center, National Chiao Tung University; and Nano-Electro-Mechanical-Systems research center, National Taiwan University, are also greatly appreciated.

REFERENCES

[1] W. Liu and M. Pecht, *IC Component Sockets*. Hoboken, NJ: Wiley-Interscience, 2004.
[2] R. S. Mroczkowski, *Electronic Connector Handbook: Theory and Applications*. New York: McGraw-Hill, 1998.
[3] T. Unno, Y. Yokohama, T. Toriyama *et al.*, "Micro connector fabricated by micro process technology," in *Proc. Int. Symp. Micro Mach. Human Sci.*, 2000, pp. 83–88.
[4] H. Toshiyoshi, Y. Mita, M. Ogawa *et al.*, "Chip level three-dimensional assembling of microsystems," in *Proc. SPIE II Int. Soc. Opt. Eng.*, vol. 3680, 1999, pp. 679–686.
[5] N. L. Tracy, R. Rothenberger, C. Copper *et al.*, "Array sockets and connectors using MicroSpring technology," in *Proc. IEEE/CPMT IEMT Symp.*, 2000, pp. 129–140.
[6] D. C. Miller, W. Zhang, and V. M. Bright, "Micromachined, flip-chip assembled, actuatable contacts for use in high density interconnection in electronics packaging," *Sens. Actuators A, Phys.*, vol. 89, no. 1/2, pp. 76–87, Mar. 2001.
[7] M. P. Larsson, "Improved contact resistance stability in a MEMS separable electrical connector," in *Proc. SPIE Int. Soc. Opt. Eng.*, 2005, vol. 6035, pp. 603 50U.1–603 50U.9.
[8] M. P. Larsson and S. Lucyszyn, "A micromachined separable RF connector fabricated using low-resistivity silicon," *J. Micromech. Microeng.*, vol. 16, no. 10, pp. 2021–2033, Aug. 2006.
[9] M. P. Larsson and R. R. A. Syms, "Self-aligning MEMS in-line separable electrical connector," *J. Microelectromech. Syst.*, vol. 13, no. 2, pp. 365–376, Apr. 2004.
[10] B.-H. Jang, P.-H. Tseng, and W. Fang, "Characterization of micro-contact properties using a novel micromachined apparatus," *J. Micromech. Microeng.*, vol. 18, no. 5, p. 055 020, Apr. 2008.
[11] R. S. Timsit, "High speed electronic connectors: A review of electrical contact properties," *IEICE Trans. Electron.*, vol. E88, no. 8, pp. 1532–1545, 2005.
[12] T.-K. Wang, T.-W. Han, and T.-L. Wu, "A novel power/ground layer using artificial substrate EBG for simultaneously switching noise suppression," *IEEE Trans. Microw. Theory Tech.*, vol. 56, no. 5, pp. 1164–1171, May 2008.
[13] C. Caloz and T. Itoh, *Electromagnetic Metamaterials: Transmission Line Theory and Microwave Applications: The Engineering Approach*. Hoboken, NJ: Wiley, 2006.
[14] M. J. Madou, *Fundamentals of Microfabrication: The Science of Miniaturization*, 2nd ed. Boca Raton, FL: CRC Press, 2002.
[15] J.-B. Wu, J.-J. Chang, M.-Y. Li *et al.*, "Characterization of diamond-like carbon coatings prepared by pulsed bias cathodic vacuum arc deposition," *Thin Solid Films*, vol. 516, no. 2–4, pp. 243–247, Dec. 2007.

Ben-Hwa Jang was born in Taipei, Taiwan, in 1970. He received the B.S. degree in mechanical engineering from Tatung Institute of Technology (renamed as Tatung University in 1999), Taipei, in 1993, and the M.S. degree from the Institute of Biomedical Engineering, National Yang-Ming University, Taipei, in 1995. He is currently working toward the Ph.D. degree at the Institute of NanoEngineering and MicroSystems, National Tsing Hua University, Hsinchu, Taiwan.

Since June 1997, he has been a Researcher with the Material and Chemical Laboratories, Industrial Technology Research Institute, Hsinchu. His current research interests include multiphysical design, analysis, modeling, and measurement for radio frequency integrated passive devices and high-speed digital systems. He also has been a Consultant to many enterprises for providing solutions on high-end connector design, high-speed printed circuit board design, electromagnetic interference, and related applications.

Hsin-Yu Huang was born in Taipei, Taiwan, in 1979. He received the B.E. degree from National Taiwan University, Taipei, in 2003, and the M.S. degree from National Taiwan Normal University, Taipei, in 2005. He is currently working toward the Ph.D. degree in the Department of Power Mechanical Engineering, National Tsing Hua University, Hsinchu, Taiwan.

His research interests include the development of novel fabrication processes, design of electrostatic actuators, microscanning mirrors, and microconnectors.

Weileun Fang (M'06) was born in Taipei, Taiwan, in 1962. He received the Ph.D. degree from Carnegie Mellon University, Pittsburgh, PA, in 1995. His doctoral research focused on the determination of the mechanical properties of thin films using micromachined structures.

In 1995, he was a Postdoctoral Researcher with the Synchrotron Radiation Research Center, Hsinchu, Taiwan. He is with National Tsing Hua University, Hsinchu, where he has been in the Department of Power Mechanical Engineering since 1996 and is currently a Professor, as well as a Faculty Member of the Institute of Nano-Engineering and MicroSystems. From June to September 1999, he was with Prof. Y.-C. Tai at California Institute of Technology, Pasadena, as a Visiting Associate. He has established a microelectromechanical systems (MEMS) testing and characterization laboratory. His current research interests include MEMS with emphasis on microfabrication/packaging technologies, micro-optical systems, microactuators, and the characterization of the mechanical properties of thin films.